Optics Communications 410 (2018) 637–642

Contents lists available at ScienceDirect

Optics Communications

journal homepage: www.elsevier.com/locate/optcom

Tunable, multiwavelength-swept fiber laser based on nematic liquid crystal device for fiber-optic electric-field sensor

Hyun Ji Lee [a,1], Sung-Jo Kim [b,*], Myeong Ock Ko [a,1], Jong-Hyun Kim [a], Min Yong Jeon [a,*]

[a] Department of Physics, Chungnam National University,99 Daehak-ro Yuseong-gu, Daejeon, 34134, Republic of Korea
[b] Center for Soft and Living matter, Institute for Basic Science, Ulsan 44919, Republic of Korea

A R T I C L E I N F O

Keywords:
Nematic liquid crystal
Wavelength-swept laser
Tunable laser
Multiwavelength fiber laser

A B S T R A C T

We propose a tunable multiwavelength-swept laser based on a nematic liquid crystal (NLC) Fabry–Perot (FP) etalon, which is embedded in the resonator of a wavelength-swept laser. We achieve the continuous wavelength tuning of the multiwavelength-swept laser by applying the electric field to the NLC FP etalon. The free spectral range of the fabricated NLC FP etalon is approximately 7.9 nm. When the electric field applied to the NLC FP etalon exceeds the threshold value (Fréedericksz threshold voltage), the output of the multiwavelength-swept laser can be tuned continuously. The tuning range of the multiwavelength-swept laser can be achieved at a value greater than 75 nm, which has a considerably wider tunable range than a conventional multiwavelength laser based on an NLC FP etalon. The slope efficiencies in the spectral and temporal domains for the tunable multiwavelength-swept laser are 22.2 nm/(mV$_{rms}$/μm) and 0.17 ms/(mV$_{rms}$/μm), respectively in the linear region. Therefore, the developed multiwavelength-swept laser based on the NLC FP etalon can be applied to an electric-field sensor. Because the wavelength measurement and time measurement have a linear relationship, the electric-field sensor can detect a rapid change in the electric-field intensity by measuring the peak change of the pulse in the temporal domain using the NLC FP etalon-based multiwavelength-swept laser.

1. Introduction

Liquid crystals (LCs) are widely used as devices in photonics technology because the effective refractive index can be easily manipulated by thermal or electromagnetic fields [1–13]. In particular, Fabry–Perot (FP) devices with an LC can be used as an optical filter in wavelength-division multiplexing optical communication systems because they can alter the transmission wavelength by applying an electric field [1–3]. The LC-based FP filter has several advantages, such as continuous tuning, a simple structure, compactness, high finesse, and a low driving voltage. On the other hand, an FP filter exhibiting a small free spectral range (FSR) can be used as a multiwavelength source. Multiwavelength lasers operating at a wavelength around 1550 nm are widely used in numerous areas of photonics technology [14–22]. An erbium-doped fiber (EDF) in the 1550-nm band is a promising gain medium for multiwavelength lasers. However, it has strong homogeneous line broadening and cross gain saturation at room temperature [23–26]. Therefore, it is difficult to achieve a stable multiwavelength laser using an EDF because of the gain competition among several lasing wavelengths. An alternative gain medium for a multiwavelength laser is a semiconductor optical amplifier (SOA) [14–16], which is evidently a better choice than EDF because of its several advantages, such as good short-term stability, multiwavelength oscillation at room temperature, and inhomogeneous linewidth broadening. The SOA-based multiwavelength operation has been demonstrated using several optical filters, including a fiber Lyot filter, a Sagnac filter, and a fiber Bragg grating-based filter [14–17]. Similarly, the LC-based FP filter can be used as a multiwavelength filter for lasers because it exhibits a small FSR. Most of the papers concerning NLC FP discuss selective-wavelength filters or multi-wavelength filters [27–30].

Recently, a method of dynamic measurement was reported for the electric-field sensor based on a wavelength-swept laser and a nematic LC (NLC) FP etalon as an optical multiwavelength tunable filter (TF) [12]. The wavelengths of the transmitted peaks of the NLC FP etalon depend on the applied electric field; therefore, their characteristics can be used for measuring the variation of the applied electric field in fiber-optic sensors. The main advantage of using a wavelength-swept laser is that it

* Corresponding authors.
E-mail addresses: sungjom@gmail.com (S.-J. Kim), myjeon@cnu.ac.kr (M.Y. Jeon).
[1] These authors contributed equally in this work.

https://doi.org/10.1016/j.optcom.2017.11.029
Received 30 June 2017; Received in revised form 6 October 2017; Accepted 10 November 2017

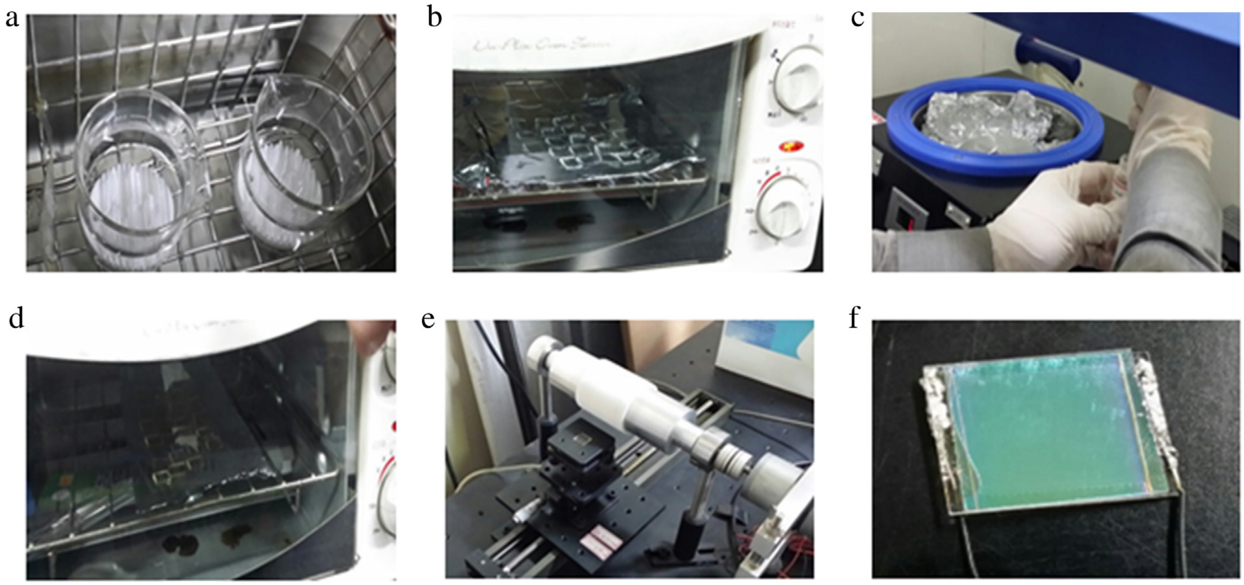

Fig. 1. Fabrication process of NLC FP etalon (a) ultrasonic cleaning, (b) baking, (c) spin coating, (d) baking, (e) rubbing, and (f) NLC FP etalon.

exhibits a one-to-one correspondence between the spectral domain and the temporal domain [12,31–33]. With the wavelength-swept laser, the dynamic variation of the electric field can be measured using a high-speed photodetector in the temporal domain.

In this paper, we propose a widely tunable multiwavelength-swept laser based on an SOA as a gain medium and an NLC FP etalon as a multiwavelength TF. Generally, a multiwavelength laser can be realized by simply inserting NLC-FP into a conventional laser resonator. However, the wavelength tuning is limited to 20–30 nm because of the narrow FSR of the NLC FP. On the other hand, when the NLC FP etalon is inserted into a wavelength-swept laser, the multiwavelength-swept laser can be continuously tuned over 75 nm by applying an electric field to the NLC FP etalon.

2. Fabrication of nematic liquid crystal device

Fig. 1 shows the fabrication process of an FP etalon for inserting the NLC. As a first step, a slide glass for a planar mirror is cleaned in an ultrasonic cleaner for eliminating the foreign substances on the glass, as shown in Fig. 1(a). We washed the slide glass using surfactant, acetone, and ethanol solutions in an ultrasonic cleaner. Subsequently, an alignment layer, where LC molecules can be oriented on the glass surface, was obtained by curing the polyamide solution. The washed slide glass was dried on a hot plate at 70 °C for 15 min, as shown in Fig. 1(b). Then, the slide glass was placed on a spin coater, the polyamide solution was spread on the glass using a pipette, and the glass was coated at approximately 3000 rpm for 30 s. After spin coating, the slide glass was cured by baking it at 70 °C for 15 min and then at 220 °C for 1 h. During this process, the polyamide became a polymer with polyimide. The next step was rubbing 10 times in a certain direction using a rubbing machine, as shown in Fig. 1(e). To form an FP etalon structure, the rubbed glass was then superimposed in antiparallel fashion. Spacers maintained a certain distance between the glasses and the mirror faces that were facing each other. The slide glass was fixed with epoxy to prevent it from moving. Fig. 1(f) shows the fabricated FP etalon with a size of 14×14 mm^2. Finally, the NLC was inserted through the gap created by the spacer using the capillary phenomenon.

Fig. 2 shows the structure of the fabricated NLC FP etalon. Commercial 4-cyano-4’-pentylbiphenyl (5CB, from Merck) was used as an NLC. The FP etalon consisted of glass substrates with an antireflection (AR) coating, indium tin oxide (ITO) layers as the electrodes, dielectric layers as the highly reflective surface, polyimide layers as the planar alignment

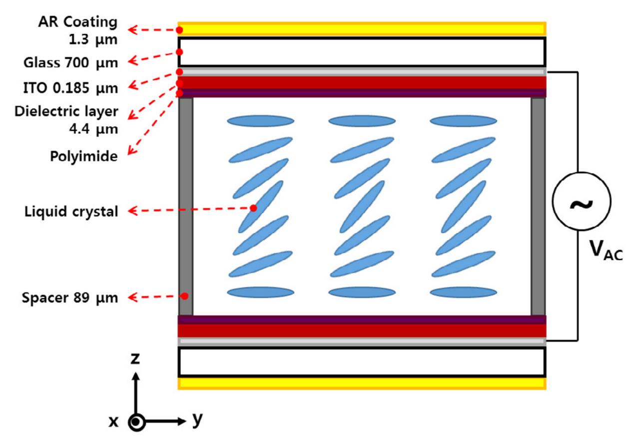

Fig. 2. Structure of the NLC FP etalon.

layers, and an LC layer. The dielectric layers were coated with Ta_2O_5 and SiO_2 materials. The AR coating was applied on the outside of the glass for eliminating the interference signals arising from the thickness of the glass. The reflectance of the dielectric layer differed depending on the wavelength, and a maximum reflectance of 84% was measured at a wavelength of 1560 nm. The thicknesses of the dielectric layer, ITO, glass, and AR coating were 4.4, 0.185, 700, and 1.3 μm, respectively. The thickness of the LC layer was approximately 89 μm after space was inserted between the polyimide layers. The NLC was homogeneously aligned along the y-axis between the polyimide layers.

The operation of the NLC FP etalon was controlled by applying an electric field using a function generator. The orientation of the NLC is along the y-axis without the electric field. With the application of the electric field along the z-axis, the director is gradually oriented along the z-axis. Therefore, the effective refractive index of the NLC changes [13]. The NLC FP etalon can be used as a wavelength filter by applying the electric field. In general, the NLC FP etalon can operate in the ordinary (n_o) and extraordinary modes (n_e) when linearly polarized light is incident on the NLC along an arbitrary polarization [12]. The transmission wavelengths of the NLC FP etalon remain unaltered for ordinary modes, whereas for extraordinary modes, they shift towards the shorter-wavelength region when the electric field is applied to

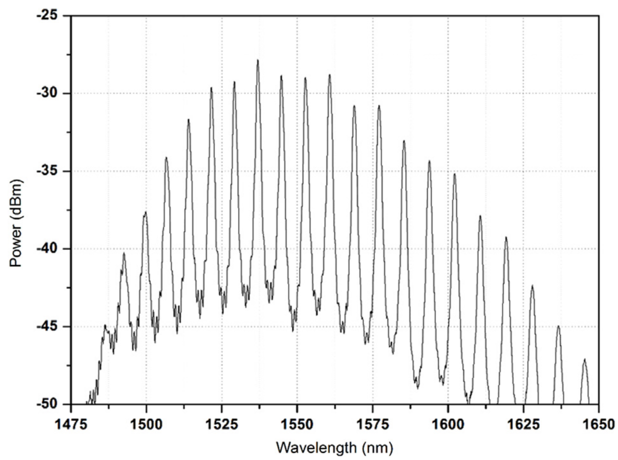

Fig. 3. Transmitted optical spectrum from the NLC FP etalon.

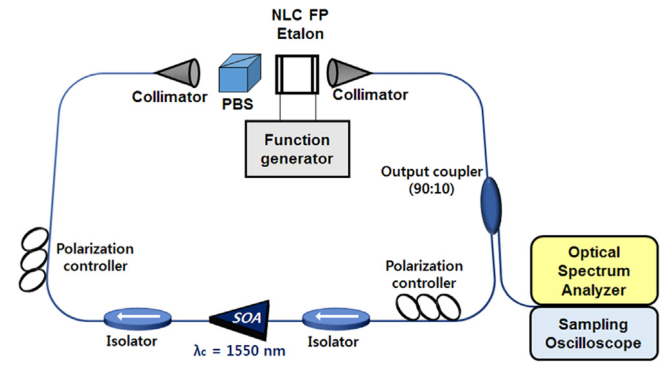

Fig. 4. Experimental setup for tunable multiwavelength fiber laser (PBS: polarization beam splitter; NLC FP etalon: nematic liquid crystal Fabry–Perot etalon; SOA: semiconductor optical amplifier).

the NLC FP etalon. Therefore, we conducted the experiments in the extraordinary mode, because the transmission wavelengths changed according to the electric field applied to the NLC FP etalon.

Fig. 3 shows the optical spectrum of the transmitted output from the NLC FP etalon when the amplified spontaneous emission (ASE) source was incident perpendicular to the NLC FP etalon surface. There are only extraordinary modes in the spectrum, because the beam was linearly polarized along the direction of the extraordinary mode of the LC molecule [12,13]. The FSR of the NLC FP etalon was approximately 7.9 nm. When the electric field applied to the NLC FP etalon exceeded the threshold value (i.e., Fréedericksz threshold voltage), the transmitted wavelengths shifted towards the shorter wavelengths. Therefore, the transmitted wavelengths from the NLC FP etalon can be tuned continuously by increasing the strength of the applied electric field.

3. Tunable multiwavelength fiber laser

Fig. 4 shows the experimental setup for a tunable multiwavelength fiber laser using an NLC FP etalon. It comprises a 1550-nm band SOA as a gain medium, two polarization controllers, two optical isolators, two fiber-optic collimators, a polarization beam splitter (PBS), a 10% output coupler, and an NLC FP etalon. The collimated output beam from the ASE source reaches the NLC FP etalon through a PBS. Polarization controller 1 adjusts the light to pass through the PBS with low loss. As the SOA has a polarization-dependent gain, polarization controller 2 adjusts the polarization of the light incident on the SOA for achieving the maximum gain. The operation of the NLC FP etalon is controlled using a function generator that applies the electric fields for tuning the transmitted wavelength peaks. Moreover, we applied an alternating-current voltage exhibiting a square-wave frequency of 10 kHz to the NLC FP etalon. The output of the multiwavelength laser was monitored using an optical spectrum analyzer (OSA) and a sampling oscilloscope.

The linearly polarized light passing through the PBS was aligned to transmit only the ordinary mode (n_o) or the extraordinary mode (n_e) of the LC molecules. Fig. 5(a) shows the optical spectra for ordinary modes (n_o) of the multiwavelength laser according to the applied electric fields. As shown in Fig. 5(a), although the intensity of the applied electric field changed, the spectra of the multiwavelength laser remained unaltered in the ordinary mode. However, when the LC molecules in the FP etalon were aligned to transmit only the extraordinary modes, the spectra of the multiwavelength laser shifted towards the shorter wavelengths according to the intensity of the applied electric field. Fig. 5(b) shows the optical spectra of the multi-wavelength laser when the electric fields applied to the NLC FP etalon were changed from 4.494 to 7.865 $mV_{rms}/\mu m$, increasing the voltage in steps of 0.112 $mV_{rms}/\mu m$. The FSR and 3-dB linewidth of the tunable multiwavelength laser were approximately 8.7 and 0.21 nm, respectively. Above the Fréedericksz threshold voltage, the directors rotated and aligned along the direction of the electric field. Because of this, the effective refractive index of the LC inside the FP etalon changed. Therefore, the multiwavelength peaks started shifting towards the shorter-wavelength region with an increase in the applied electric field [12]. The intensities of the output of multiple wavelengths in the Fig. 5(b) are not the same. It is very difficult to obtain the same output of multiple wavelengths when the NLC FP etalon is inserted into the laser cavity. Fig. 5(c) shows a plot of the tunable outputs of the multiwavelength laser, which corresponds to Fig. 5(b). The lasing wavelengths shifted towards the shorter wavelengths with an increase in the applied electric field. A wavelength tuning of greater than 20 nm can be achieved for the multiwavelength peaks. Above the Fréedericksz threshold voltage, the wavelength changes linearly as the voltage increases and gradually becomes nonlinear, resulting in saturation. This is the same phenomenon whereby the effective refractive index of the LC is changed by applying an electric field to the LC in the FP etalon [13]. However, when the intensity of the electric field changes from 4.494 to 7.865 $mV_{rms}/\mu m$, the wavelength tuning changes almost linearly because the wavelength-tuning range is within the gain band. The slope efficiency for the tunable multiwavelength laser is 22.2 $nm/(mV_{rms}/\mu m)$.

4. Tunable multiwavelength-swept fiber laser

To achieve a wide range of wavelength tunability, the NLC FP etalon is inserted into a wavelength-swept laser. Fig. 6 shows the experimental setup for a tunable multiwavelength-swept laser using the NLC FP etalon. It is similar to Fig. 4, except that the fiber FP (FFP)-TF (Lambda Quest Inc.) is inside the laser cavity. Therefore, the wavelength-swept laser can be operated by eliminating the NLC FP etalon in the laser cavity. It is a conventional wavelength-swept laser based on the FFP-TF [31]. The scanning speed and the 3-dB scanning bandwidth of the conventional wavelength-swept laser are 210 Hz and 100 nm, respectively. It is possible to achieve a tunable multiwavelength-swept laser by inserting the NLC FP etalon into the laser cavity. There are only extraordinary wavelength modes in the laser cavity, because the input beam is adjusted using a linearly polarized beam along the direction of the extraordinary mode of the LC molecules. The outputs of the multiwavelength-swept laser from the 10% output coupler are monitored using an OSA and a sampling oscilloscope. All instruments are controlled by a LabView program via a general-purpose interface bus.

Fig. 7(a) shows the optical spectrum obtained using the multiwavelength-swept laser without an electric field applied to the NLC FP etalon. There are only extraordinary modes in the optical spectrum,

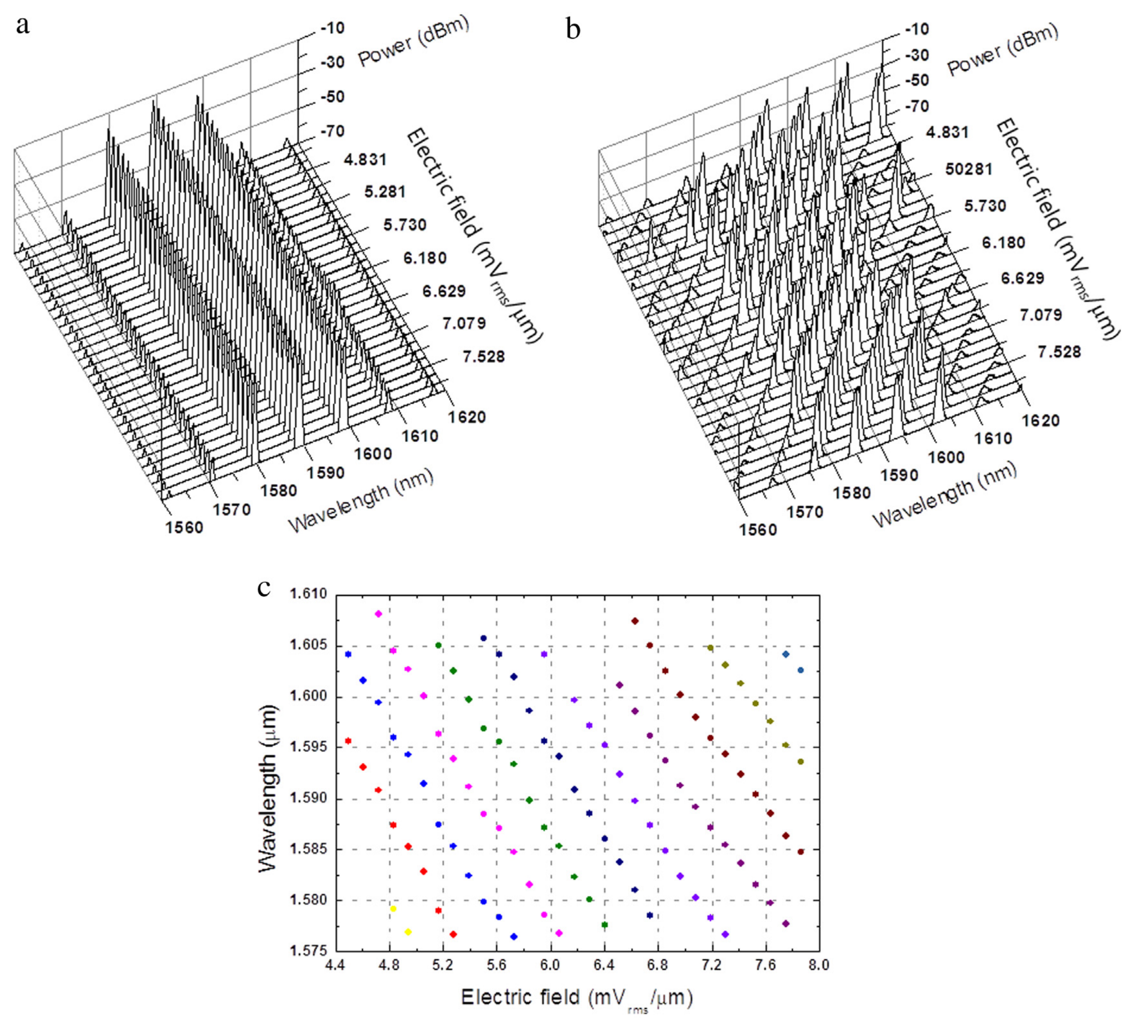

Fig. 5. (a) Optical spectra for ordinary modes, (b) optical spectra for extraordinary modes, and (c) plots of the tunable outputs of the multiwavelength laser for an applied electric field varying from 4.494 to 7.865 mV$_{rms}$/μm in steps of 0.121 mV$_{rms}$/μm.

because the LC molecules in the FP etalon are aligned to transmit only the extraordinary modes. The multiwavelength-swept laser can be measured in the temporal domain using a photodetector because the spectral outputs in the OSA and the temporal outputs in the sampling oscilloscope are correlated. Fig. 7(b) shows the pulse peaks from the multiwavelength-swept laser in the temporal domain. The pulses in Fig. 7(b) precisely correspond to those in Fig. 7(a). Their peak intensities are almost identical, as shown in Fig. 7.

Fig. 8(a) shows the optical spectra of the tunable multiwavelength-swept laser when the electric field applied to the NLC FP etalon changed from 4.494 to 7.865 mV$_{rms}$/μm, increasing the electric field in steps of 0.112 mV$_{rms}$/μm. The output of the multiwavelength-swept laser can be tuned continuously to a value greater than 75 nm. The 3-dB bandwidth of each wavelength is approximately 0.6 nm. The outputs of the multiwavelength-swept laser shifted towards the shorter wavelengths with an increase in the applied electric field. Fig. 8(b) plots the temporal outputs from the tunable multiwavelength-swept laser, which correspond to Fig. 8(a). For the electric-field intensity range of 4.494 to 7.865 mV$_{rms}$/μm, the spectral and temporal outputs change almost linearly because the wavelength-tuning range is within the gain band of ~100 nm. The slope efficiencies in the spectral and temporal domains for the tunable multiwavelength-swept laser are 22.2 nm/(mV$_{rms}$/μm) and 0.17 ms/(mV$_{rms}$/μm), respectively. The measurement resolution for an electric-field sensor using a multiwavelength laser depends on the 3-dB bandwidth.

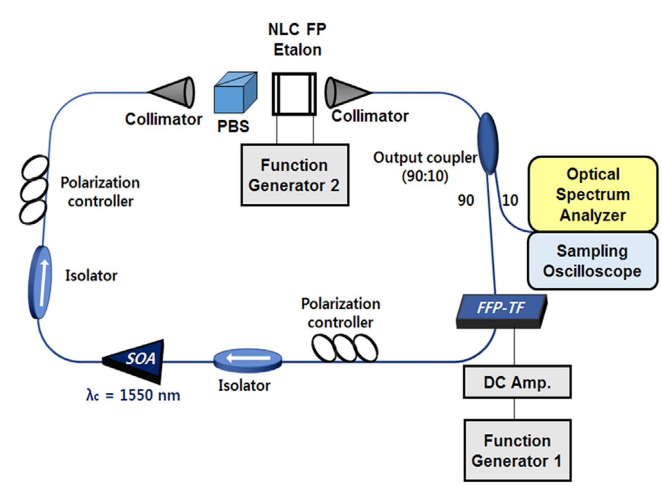

Fig. 6. Schematic diagram of experimental setup.

5. Summary

We successfully demonstrated a tunable multiwavelength-swept laser based on an SOA using a NLC FP etalon as an optical multiwavelength tunable filter. A wide tuning range was achieved at a value

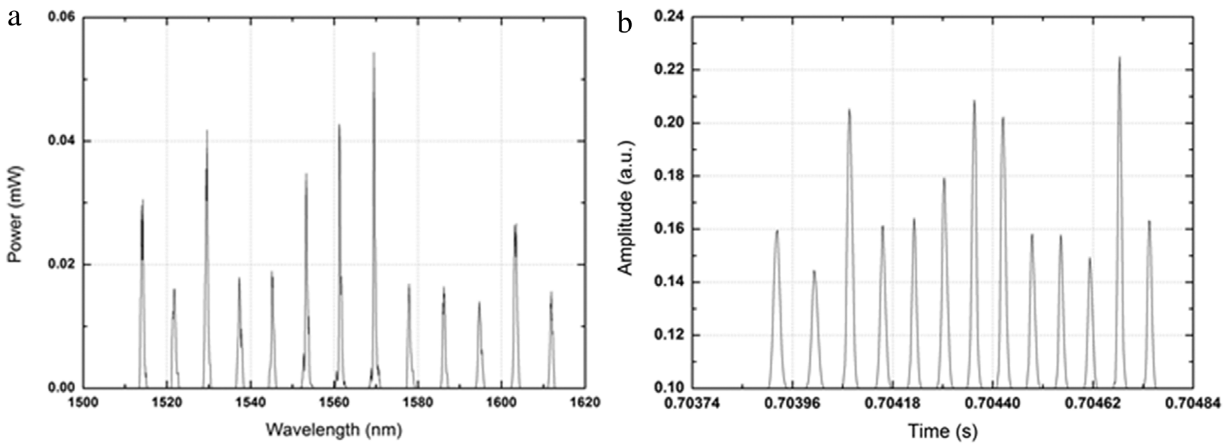

Fig. 7. Outputs of multiwavelength-swept laser: (a) optical spectrum and (b) pulses position in temporal domain.

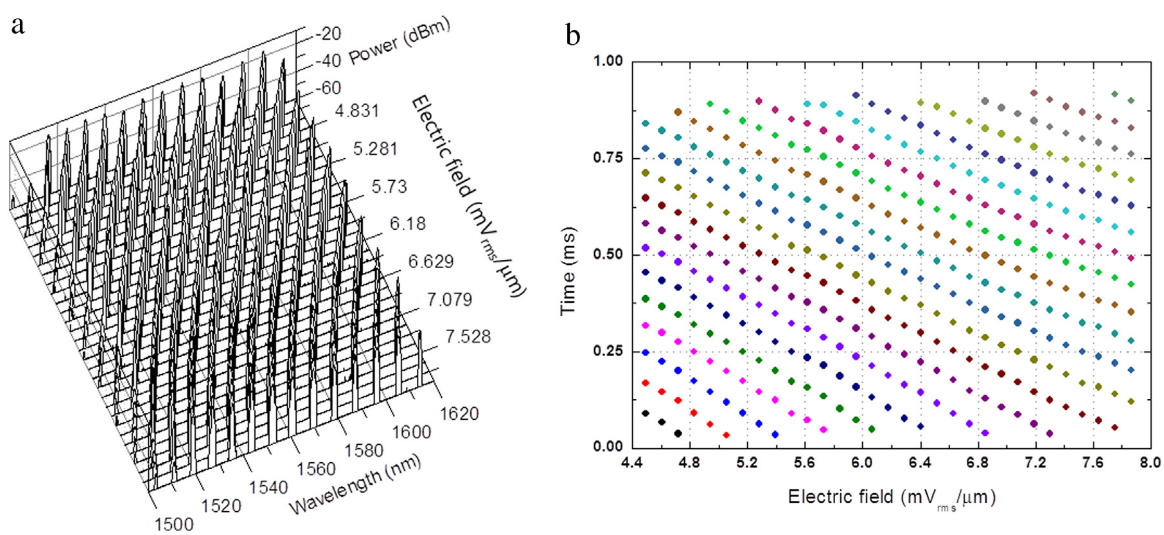

Fig. 8. (a) Optical spectra for extraordinary modes and (b) plots of the tunable outputs of the multiwavelength laser for the applied electric field varying from 4.494 to 7.865 $mV_{rms}/\mu m$ in steps of 0.121 $mV_{rms}/\mu m$.

greater than 75 nm, approximately in the 1550-nm band. The 3-dB bandwidth of each wavelength was approximately 0.6 nm. Continuous multiwavelength tuning of the multiwavelength-swept laser was achieved by applying the electric field to the NLC FP etalon. When the electric field applied to the NLC FP etalon exceeded the threshold value (Fréedericksz threshold voltage), the output of the multiwavelength-swept laser could be tuned. The outputs of the multiwavelength-swept laser shifted towards the shorter wavelengths with an increase in the applied electric field. For an electric-field intensity range of 4.494 to 7.865 $mV_{rms}/\mu m$, the wavelength tuning changed almost linearly because the wavelength-tuning range was within the gain band of the laser. The slope efficiencies in the spectral and temporal domains for the tunable multiwavelength-swept laser were 22.2 nm/($mV_{rms}/\mu m$) and 0.17 ms/($mV_{rms}/\mu m$), respectively. Therefore, the multiwavelength-swept laser based on the NLC FP etalon can be applied to an electric-field sensor. The advantage of a wavelength-swept laser is that it can measure the same change in the temporal domain instead of measuring the wavelength change in the spectral domain. Therefore, an electric-field sensor with rapid change in the electric-field intensity can be achieved by measuring the peak change of the pulse in the temporal domain using the LC-based multiwavelength-swept laser.

Acknowledgments

This research was supported by The Leading Human Resource Training Program of Regional Neo industry through the National Research Foundation of Korea (NRF) funded by the Ministry of Science, ICT and future Planning (NRF-2016H1D5A1909597) and by Basic Science Research Program through the National Research Foundation of Korea (NRF) funded by the Ministry of Science, ICT and future Planning (NRF-2014R1A2A1A11051152 and NRF-2017R1A2B4008212).

References

[1] Y. Bao, A. Sneh, K. Hsu, K.M. Johnson, J.-Y. Liu, C.M. Miller, Y. Monta, M.B. McClain, High-speed liquid crystal fiber Fabry–Perot tunable filter, IEEE Photon. Tech. Lett. 8 (1996) 1190–1192.
[2] J.E. Stockley, G.D. Sharp, K.M. Johnson, Fabry Perot etalon with polymer cholesteric liquid-crystal mirrors, Opt. Lett. 24 (1999) 55–57.
[3] Z.Z. Zhuang, J.S. Patel, Y.J. Kim, Behavior of the cholesteric liquid-crystal Fabry–Perot cavity in the Bragg reflection band, Phys. Rev. Lett. 84 (2000) 1168–1171.
[4] O. Aharon, I. Abdulhalim, Liquid crystal Lyot tunable filter with extended free spectral range, Opt. Express 17 (2009) 11426–11433.
[5] O. Aharon, I. Abdulhalim, Tunable optical filter having a large dynamic range, Opt. Lett. 34 (2009) 2114–2116.
[6] Z. Zheng, G. Yang, H. Li, X. Liu, Three-stage Fabry–Perot liquid crystal tunable filter with extended spectral range, Opt. Express 19 (2011) 2158–2164.

[7] D.F. Bendimerad, B.-E. Benkelfat, R. Hamdi, Y. Gottesman, O. Seddiki, B. Vinouze, Channel equalization and bandwidth tuning using a LC-based tunable hybrid birefringent filter, J. Lightwave Technol. 30 (2012) 2103–2109.
[8] S. Isaacs, F. Placido, I. Abdulhalim, Investigation of liquid crystal Fabry–Perot tunable filters: design, fabrication, and polarization independence, Appl. Opt. 53 (2014) H91–H101.
[9] Y. Semenova, G. Farrell, G. Rajan, Fabry–Perot liquid crystal tunable filter for interrogation of multiple fibre Bragg grating sensors, Proc. SPIE 6587 (2007) 658714.
[10] J. Beeckman, K. Neyts, P.J.M. Vanbrabant, Liquid-crystal photonic applications, Opt. Eng. 50 (2011) 081202.
[11] Y. August, A. Stern, Compressive sensing spectrometry based on liquid crystal devices, Opt. Lett. 38 (2013) 4996–4999.
[12] M.O. Ko, S.-J. Kim, J.-H. Kim, B.W. Lee, M.Y. Jeon, Dynamic measurement for electric field sensor based on wavelength-swept laser, Opt. Express 22 (2014) 16139–16147.
[13] M.O. Ko, S.-J. Kim, J.-H. Kim, B.W. Lee, M.Y. Jeon, Measurement of effective refractive index of nematic liquid crystal in Fabry–Perot etalon, J. Opt. Soc. Korea 19 (2015) 346–350.
[14] S. Kim, J. Kwon, S. Kim, B. Lee, Multiplexed strain sensor using fiber grating tuned fiber laser with a semiconductor optical amplifier, IEEE Photon. Technol. Lett 13 (2001) 350–351.
[15] Y.W. Lee, J. Jung, B. Lee, Multiwavelength-switchable SOA-fiber ring laser based on polarization-maintaining fiber loop mirror and polarization beam splitter, IEEE Photon. Technol. Lett. 16 (2004) 54–56.
[16] M.A. Ummy, N. Madamopoulos, A. Joyo, M. Kouar, R. Dorsinville, Tunable multi-wavelength SOA based linear cavity dual-output port fiber laser using Lyot-Sagnac loop mirror, Opt. Express 19 (2011) 3202–3211.
[17] S.-C. Chen, J.-D. Lin, C.-R. Lee, S.-J. Hwang, Multi-wavelength laser tuning based on cholesteric liquid crystals with nanoparticles, J. Phys. D Appl. Phys. 49 (2016) 16502.
[18] K.K. Qureshi, H.Y. Tam, W.H. Chung, P.K.A. Wai, Multiwavelength laser source using linear optical amplifier, IEEE Photonics Technol. Lett. 17 (2005) 1611–1613.
[19] T. Wang, X. Miao, X. Zhou, S. Qian, Tunable multiwavelength fiber laser based on a double Sagnac HiBi fiber loop, Appl. Opt. 51 (2012) C111–C116.
[20] S. Qin, D. Chen, Y. Tang, S. He, Stable and uniform multi-wavelength fiber laser based on hybrid Raman and Erbium-doped fiber gains, Opt. Express 14 (2006) 10522–10527.
[21] Y. Luo, L. Xia, Q. Sun, W. Li, Y. Ran, D. Liu, Multi-wavelength fiber laser based on self-seed light amplification and wavelength-dependent gain, Opt. Comm. 338 (2015) 336–339.
[22] P. Wang, L. Wang, G. Shi, T. He, H. Li, Y. Liu, Stable multi-wavelength fiber laser with single-mode fiber in a Sagnac loop, Appl. Opt. 55 (2016) 3339–3342.
[23] N. Park, P.F. Wysocki, 24-line multiwavelength operation of erbium-doped fiber-ring laser, IEEE Photon. Technol. Lett. 8 (1996) 1459–1461.
[24] S. Pan, C. Lou, Y. Gao, Multiwavelength erbium-doped fiber laser based on inhomogeneous loss mechanism by use of a highly nonlinear fiber and a Fabry–Perot filter, Opt. Express 14 (2006) 1113–1118.
[25] P. Wang, D. Weng, K. Li, Y. Liu, X. Yu, X. Zhou, Multi-wavelength erbium-doped fiber laser based on four-wave-mixing effect in single mode fiber and high nonlinear fiber, Opt. Express 21 (2013) 12570–12578.
[26] Z.C. Tiu, H. Ahmad, A. Zarei, S.W. Harun, Generation of multi-wavelength erbium-doped fiber laser by using $MoSe_2$ thin film as nonlinear medium and stabilizer, Chin. Opt. Lett. 14 (2016) 041901.
[27] M.W. Maeda, J.S. Patel, D.A. Smith, C. Lin, M.A. Saifi, A. Von Lehman, An electronically tunable fiber laser with a liquid-crystal etalon filter as the wavelength-tuning element, IEEE Photon. Technol. Lett. 2 (1990) 787–789.
[28] K. Hirabayshi, H. Tsuda, T. Kurokawa, Tunable liquid-crystal Fabry–Perot interferometer filter for wavelength-devision multiplexing communication systems, J. Lightwave. Technol. 11 (1993) 2033–2043.
[29] Shadi A. Alboon, Robert G. Lindquist, Flat top liquid crystal tunable filter using coupled Fabry–Perot cavities, Opt. Express 16 (2008) 231–236.
[30] J. Cos, J. Ferre-Borrull, J. Pallares, L.F. Marsal, Tunable Fabry–Perot filters based on one-dimensional photonic crystals with liquid crystal components, Opt. Comm. 282 (2009) 1220–1225.
[31] E.J. Jung, C.-S. Kim, M.Y. Jeong, M.K. Kim, M.Y. Jeon, W. Jung, Z. Chen, Characterization of FBG sensor interrogation based on a FDML wavelength swept laser, Opt. Express 16 (2008) 16552–16560.
[32] Y.S. Kwon, M.O. Ko, M.S. Jung, I.G. Park, N. Kim, S.-P. Han, H.-C. Ryu, K.H. Park, M.Y. Jeon, Dynamic sensor interrogation using wavelength-swept laser with a polygon-scanner-based wavelength filter, Sensors 13 (2013) 9669–9678.
[33] H.D. Lee, G.H. Kim, T.J. Eom, M.Y. Jeong, C.-S. Kim, Linearized wavelength interrogation system of fiber bragg grating strain sensor based on wavelength-swept active mode locking fiber laser, J. Lightwave Technol. 33 (2015) 2617–2622.